Service performance of nanopins based on branched carbon nanotubes

Zhong-Qiang Zhang[1,2] ✉, *Jun Zhong*[1], *Zhen Liu*[3], *Guang-Gui Cheng*[1], *Jian-Ning Ding*[2]

[1]*Micro/Nano Science and Technology Center, Jiangsu University, Zhenjiang 212013, People's Republic of China*
[2]*Jiangsu Collaborative Innovation Center of Photovoltaic Science and Engineering, Changzhou University, Changzhou 213164, People's Republic of China*
[3]*School of Naval Architecture and Ocean Engineering, Jiangsu University of Science and Technology, Zhenjiang 212003, People's Republic of China*
✉ *E-mail: zhangzq@mail.ujs.edu.cn*

Published in Micro & Nano Letters; Received on 28th March 2017; Revised on 13th June 2017; Accepted on 22nd June 2017

Service performance of nanopins based on different branched carbon nanotubes (CNTs) including the 45° Y-type CNT, the 45° V-type CNT, the 90° Y-type CNT, and the T-type CNT have been investigated using classical molecular dynamics simulations. The Y-type CNT is the most cost-effective while there is adequate room to improve its service performance. The installed V-type CNT always has a trend of leaving from the silicon hole, and thus it would better be used with another nanopin cooperatively. For the 90° Y-type CNT, the installation resistance and the unloading force are almost in the same order of magnitude while the installation in pushing approach is relatively easier than that in pulling approach. Interestingly, the attraction between the silicon hole and the T-type CNT can mislead the branch, resulting in the failed installation of the T-type CNT consequently.

1. Introduction: In the past half century, great advances have been achieved in the field of nanometre materials, and the design and application of the nanodevices have become one of the most popular hotspots [1]. With the various nanodevices springing up like mushrooms, one of the increasingly crucial problems is to develop new structures and processing methods for the integration of various nanodevices.

Since the bottom-up assembly approach was proposed by Feynman in 1959, there has been a great assumption of fabricating materials and devices atom by atom. Nevertheless, until the scanning tunnel microscope (STM) was invented, ultimately we can precisely observe and manipulate a single atom. The first attempt of reconstruction on Si (111) surface in real space was reported in 1983 [2], and then it raised the tide of researches on atomic manipulation. Subsequently, it was found that the low temperature requirement is one of the significant limitations, especially for the relatively complex structures [3]. Although the vertical atomic manipulation can somewhat facilitate the operation, force field analysis [4] shows that the STM tip lowers the diffusion barrier and the termination of the tip determines the lateral manipulation force threshold, consequently affecting the final results of atomic manipulation. Furthermore, the atomic manipulation in other operating conditions such as a single atom in an ionic crystal surface [5] is quite difficult. As a result, some novel mechanisms of atomic manipulation were proposed, such as thermally activated electron attachment [6], generalised magicity of nanoclusters [7], electronic excitation of the atom or molecule [8] and so forth. Recently, IBM Research has firstly demonstrated a reversible Bergman cyclisation by the means of atom manipulation [9], which is considered as a new height in atomic manipulation, looking forward to opening up a new field of radical chemistry for on-surface reactions by atomic manipulation.

Self-assembly, originally applied to nanoparticles [10, 11], is another alternative approach to the bottom-up assembly. A typical example is drying-mediated self-assembly [12], i.e. evolving the mesostructures or complex composites as the solvent evaporates, similar to the crystallisation process. Nevertheless, this kind of self-assembly is distinctly sensitive to the solvent, and evaporation-crystallisation process is hard to control. As a result, the application of the self-assembled materials is considerably limited, especially for the nanostructured devices. Fortunately, the progress in biochemical field brings us a new ground – supramolecular self-assembly. Various functional groups, such as amphiphilic groups [13–15], can make up the block copolymers [16–18], dendrimers [19], hierarchical structures [20] and so on by coordination chemistry. Following the example of amino acid, supramolecular self-assembly is expected to form polymer molecular groups and consequently realise superstructure or nanorobots. However, except the existing biomolecule, the synthetic polymer molecules have many limitations in application. For instance, supramolecular self-assembly depends strongly on the solvent structure [21]. Although the assistance of the enzyme [22] or other surfactants [23] can catalyse the desired reaction, it is far from enough for designing or programming the self-assembly pathways. Moreover, molecular recognition plays an important role in the synthesis and application of the synthetic polymer molecules [24]. However, obviously, there is a long way to go before the synthetic polymers can recognise each other accurately.

Apparently, the atomic manipulation and molecular self-assembly are not ready yet, while micro/nanomanufacturing technology is still considered as a powerful tool to realise the simple integration. However, most of the nanoscale integrations for now refer to the integrated arrays of carbon nanotubes (CNTs) [25], nanorods [26], nanogaps [27], nanoholes [28] and so on, rather than the connection of nanodevices. One exception is that the first CNT computer [29], fabricated entirely from CNT field-effect transistors (CNFETs), has realised the integration of the molecular-level electronic devices, but the integration approaches including the deposition and etch and so on are not exactly suitable for the nanodevices in other service environment. As a result, more complex nanodevices such as mechanical devices [30, 31], energy-storage devices [32, 33], and nanofluidic devices [34–36] still remain as individuals. Therefore, a new connection mode for mass assembly of nanodevices is necessary. Here, considering the incredible properties of CNTs, we demonstrate four types of nanopin models based on CNTs for part fixation and connection, and attempt to specify their performance and applicability.

2. Model and method: Considering the difficulties in experimental operation and characterisation of nanotubes [37], the classical molecular dynamics (MD) simulations are used to observe and

doi: 10.1049/mnl.2017.0188

measure their performance in fixity, characterised by the maximum unloading resistance. In this work, there are four typical nanopin models based on armchair (12, 12) SWCNTs, i.e. 45° Y-type CNT, 45° V-type CNT, 90° Y-type CNT, and T-type CNT separately, as illustrated in Fig. 1. For the 45° Y-type CNT considered here, the length of the left end is 30 Å and the height of the branch is 40 Å. The 45° V-type CNT is developed from the 45° Y-type CNT by extending the branch to a length of ~200 Å, approaching the length of the trunk CNT. Moreover, the Y-type CNT with a 90° angle is a special example with two fixed modes, represented by 90° Y-type CNT and T-type CNT, respectively, as shown in Figs. 1*c* and *d*. The branches of them have the same height of 40 Å, i.e. $h_{CD} = h_{EF} = 40$ Å $= h_{AB}$, to fasten the hole parts. As the nanopins are used as the shaft parts, a silicon component with a through hole is still considered as the typical hole part. The silicon component is briefly assumed to be of a diamond cubic crystal structure, with the size of 100 × 120 × 40 Å in x, y and z directions. Particularly, the installation process of the 45° Y-type CNT is schematically shown in Fig. 1*e*.

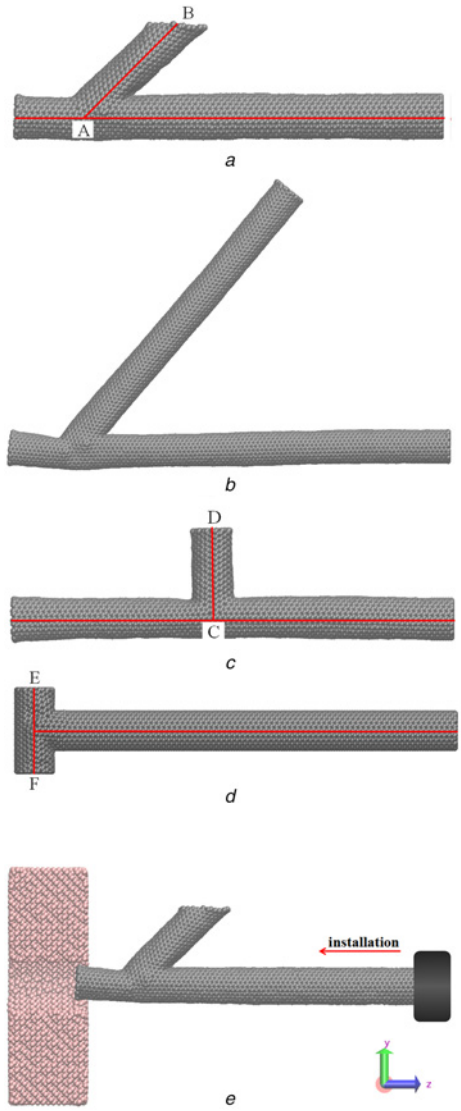

Fig. 1 *Atomic models of*
a 45° Y-type CNT
b 45° V-type CNT
c 90° Y-type CNT, and
d T-type CNT. All the nanopin models are made up of armchair (12, 12) SWCNTs. The length of trunk CNTs is 200–250 Å, while the branches of 45° Y-type CNT, 90° Y-type CNT, and T-type CNT have the same height of 40 Å
e Installation of the 45° Y-type CNT. The pink is the silicon component with a through hole, and the black represents a nanocomponent with this nanopin

Although MD simulation produces a result not as accurate as the results produced by Car–Parrinello MD or density functional theory [38], classical MD simulation has high computational efficiency in simulating the large-scale systems and can also reveal the general mechanical properties. In the field of solid mechanics, classical MD can simulate a system with the spatial scale below nanometres and the time scale of picoseconds [39], therefore, using the MD software LAMMPS, the MD models here are simulated in an *NVT* ensemble with a timestep of 1 fs (10^{-15} s) to observe the details, while all the simulation data are time-averaged in 10 ps. Since the service performance of the nanopins, i.e. comprehensive performance during the loading/unloading processes, is not sensitive to the temperature and velocity in normal range [40], 300 K is briefly considered as the kinetic temperature of the nanopin systems, and 10 m/s is considered as the moving velocity of the nanopins in the following simulations. The equilibration is achieved by relaxing the nanopin systems for 400 ps before the loading/unloading processes, and there is always a moving distance of ~40 Å to achieve the stable state of the moving nanopins. For the proposed nanopin systems, all the CNT models contain thousands of carbon atoms, belonging to the large-scale CNTs, and there are over 20,000 silicon atoms on the silicon component in a diamond cubic crystal structure. Therefore, the Adaptive Intermolecular Reactive Empirical Bond Order potential is applied for the C–C bonds, and the Stillinger–Weber (SW) potential is applied for Si–Si bonds. The Lennard–Jones (LJ) potential is applied for van der Waals between carbon and silicon atoms, and the parameters are $\varepsilon = 3.466$ meV and $\sigma = 2.8$ Å [41–43]. In order to facilitate the comparison and reveal the general patterns of the proposed models, the axial loading/unloading forces of the nanopins are the main objects to be observed in the following simulations.

3. Results and discussion: Although the nanopins are assumed to be loaded and unloaded with the same velocity under the identical temperature, these four kinds of nanopins may have different appropriate gaps owing to their different branched structures. Hence, a series of MD simulations with different gaps between the tube wall of the branched CNT and the internal surface of the silicon hole in the proposed model (represented by ΔR) are performed on each nanopin to qualitatively characterise the loading/unloading patterns and evaluate their performance and applicability.

As the fixed mode is similar to the macrobarb, the 45° Y-type CNT is firstly examined with the gaps ranging from 0.864 to 7.864 Å. For the case of $\Delta R = 0.864$ Å, the silicon hole is too small to allow the 45° Y-type CNT to pass through, as illustrated in Fig. 2. Fig. 3 shows the variation of the axial force of the 45° Y-type CNT exerted by the silicon component during the loading/unloading processes. Obviously, the loading and unloading force and the corresponding deformation of the 45° Y-type CNT is

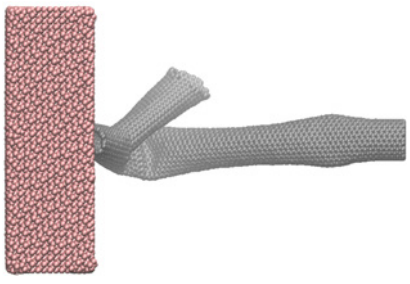

Fig. 2 *In the case of $\Delta R = 0.864$ Å, 45° Y-type CNT failed to pass through the silicon hole and the great bending deformation occurred*

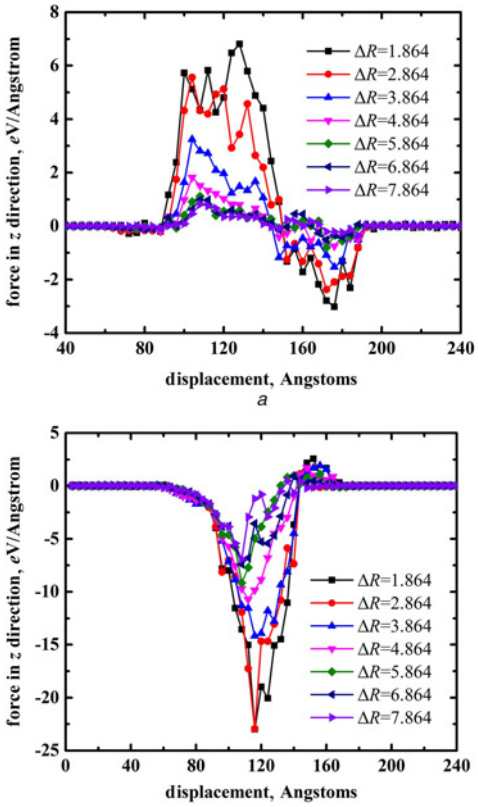

Fig. 3 *Force of the 45° Y-type CNT in z-direction as a function of the moving displacement in the*
a Loading processes and
b Unloading processes

increased with decreasing the gap, and the oscillation in the installing stage and recovering stage become larger gradually. Compared with the installation, the 45° Y-type CNT experiences a much larger resistance force in the uninstallation, which is more than three times of the installation resistance. Particularly, for the larger gap of $\Delta R \geq 5.864$ Å, the resistance force between the 45° Y-type CNT and the silicon component in the uninstallation is ~8 times of that in the installation. By contrast, the fixity of the 45° Y-type CNT in the cases of $\Delta R = 1.864$ Å and $\Delta R = 2.864$ Å is considerably extraordinary. To address this, two typical configurations of the 45° Y-type CNT in the cases of $\Delta R = 2.864$ Å and $\Delta R = 3.864$ Å are taken at the moving displacement of 116 Å in Fig. 4, corresponding to the maximum resistances during the uninstallation in Fig. 3*b*. It can be found that there is a kind of microstructure

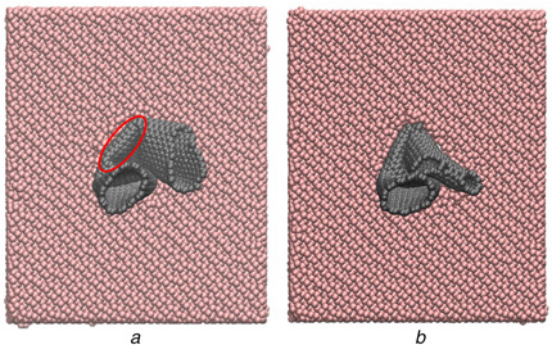

Fig. 4 *Configurations of the 45° Y-type CNT in the cases of*
a $\Delta R = 2.864$ Å and
b $\Delta R = 3.864$ Å are taken at the moving displacement of 116 Å, corresponding to the maximum resistances during the unloading processes in Fig. 3*b*

similar to the stiffening rib in the case of $\Delta R = 2.864$ Å, as ringed by a red circle in Fig. 4*a*, restraining the further adaptive deformation of the branch tube, and thus the branch can bear relatively more resistance derived from the silicon component. As for the 45° Y-type CNT in the case of $\Delta R = 3.864$ Å, the branch suffers a similar deformation with a distinct cambered surface near the joint (see Fig. 4*b*), giving no evident resistance to the adaptive deformation of the branch, and thus the nanopin has a relatively lower bearing capacity. Therefore, if the stiffening structure of the branch tube can be artificially programmed, the fixity of the Y-type CNTs will be further enhanced.

On the other hand, with a special structure like the split pin at macroscale, the 45° V-type CNT has a unique fixed mode. MD simulations with different gaps are conducted to examine the performance of the 45° V-type CNT. Fig. 5 plots the axial force of the 45° V-type CNT as a function of the displacement in the loading/unloading processes. Apparently, compared with the 45° Y-type CNT, the longer branch can lead to a larger installation resistance with larger oscillation (see Figs. 5*a* and 3*a*). However, it is considerably disappointing that the installed V-type CNT always has a trend of leaving from the silicon hole. As shown in Fig. 5*b*, the 45° V-type CNT with the smaller gaps ($\Delta R = 1.864$, 2.864 and 3.864 Å) undergoes a small resistance with relatively large oscillation in the early phase of the unloading processes and an evidently positive force in the later phase, which facilitates the uninstallation. On the contrary, for the larger gaps ($\Delta R = 5.864$, 6.864 and 7.864 Å), the force the silicon component exerted on the 45° V-type CNT is slightly larger than zero at the beginning of the unloading processes, while it turns into a negative value at the moving displacement of ~120 Å, contributing to the weak unloading force. Particularly, the case of $\Delta R = 4.864$ Å is considered as somewhere in between, with the axial force of the 45° V-type CNT vibrating around the level of zero.

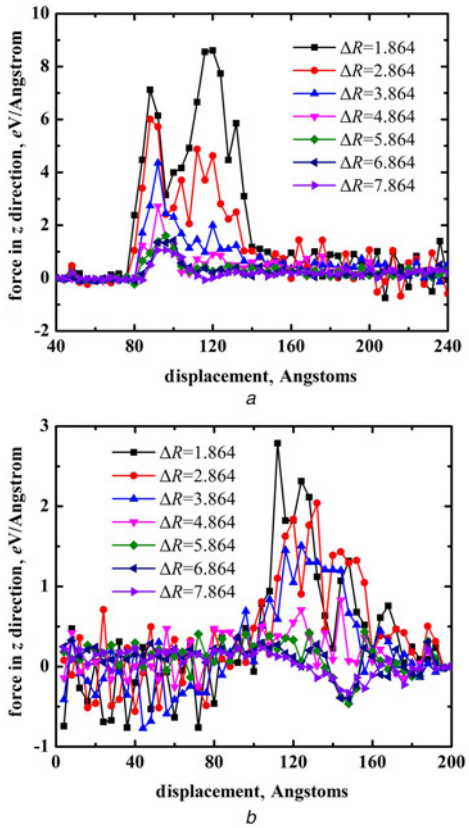

Fig. 5 *Axial force on the 45° V-type CNT as a function of the moving displacement in the*
a Lading processes
b Unloading processes

doi: 10.1049/mnl.2017.0188

To explain these phenomena, several typical configurations of the 45° V-type CNT in the loading/loading processes are taken in Fig. 6. Interestingly, the 45° V-type CNT with smaller gap of $\Delta R = 1.864$ Å at the displacement of 112 Å, which has a distinct positive force (see Fig. 5*b*), is at the time of the joint passing through the silicon hole and the large deformation recovering (see Fig. 6*a*). Therefore, the deformed joint diminishes the conflict between the 45° V-type CNT and the silicon component during the uninstallation, while the recovery of the deformed 45° V-type CNT with the smaller gaps can lead to a distinct repulsion on the right side of the silicon hole, and thus the 45° V-type CNT suffers a positive force exerted by the silicon component. By contrast, the 45° V-type CNT with larger gap of $\Delta R = 5.864$ Å at the displacement of 148 Å, which has a distinct negative force (see Fig. 5*b*), is at the time of the joint leaving from the silicon hole (see Fig. 6*b*). In other words, the unloading force is strengthened by the attraction between the silicon component and the joint, and the attraction becomes smaller as the gap further increases (see Fig. 5*b*). In addition, during the early phase of the unloading process, there is no change in the total number of the carbon atoms passing through the silicon hole (see Fig. 6*c*), and thus we attribute the difference in the early phase to the radial morphology changes of the trunk CNT and the branch CNT. The smaller gaps can lead to the continuous larger deformation of the CNTs, while the radial stability prevents the occurrence of deformation. Therefore, the smaller gaps ($\Delta R = 1.864$, 2.864 and 3.864 Å) have the slight unloading resistance force with the larger oscillation (see Fig. 5*b*) in the early phase of the unloading processes. By contrast, the deformation of the 45° V-type CNT with larger gaps ($\Delta R \geq 5.864$ Å) is much smaller without impacting the radial stability, and the recovery of the small deformation still can lead to the slight repulsion exerted by the right side of the silicon hole (see Fig. 5*b*). Overall, the 45° V-type CNT cannot effectively fasten the silicon component on its own. However, due to the unique fixed mode similar to split pin, the joint can be locked by another nanopin after the 45° V-type CNT is installed. Therefore, the 45° V-type CNT should be used cooperatively with other nanopins.

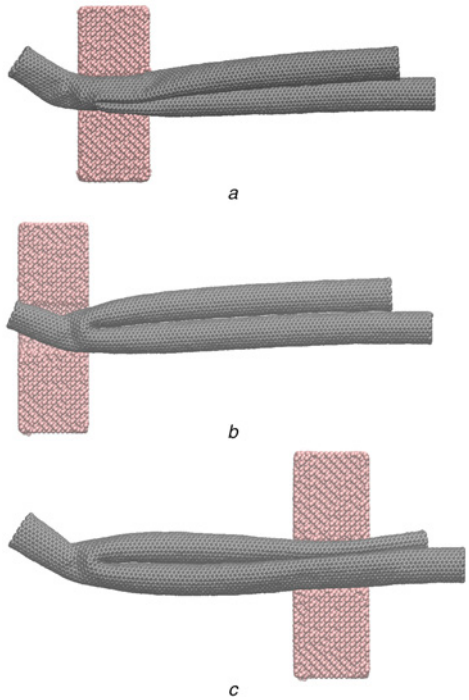

Fig. 6 *Configurations of the 45° V-type CNT*
a With $\Delta R = 1.864$ Å at the displacement of 112 Å
b With $\Delta R = 5.864$ Å at the displacement of 148 Å and
c With $\Delta R = 4.864$ Å at the initial position in the unloading processes

The 90° Y-type CNT is another special case among the Y-junction CNTs owing to the unique structure similar to the T-type CNTs. As installed/uninstalled like the former two, the 90° Y-type CNT is expected to meet the same resistance force in the loading and unloading processes because of its symmetrical structure. Fig. 7 shows the variation of the axial force of the 90° Y-type CNT during the loading/unloading processes, with the gaps ranging from 2.864 to 9.864 Å. Surprisingly, the unloading force is always larger than the installation resistance for the 90° Y-type CNT. Actually, the inserting end and the control end of the 90° Y-type CNT have the similar length, and thus the loading/unloading processes can be seen as two typical installation methods, i.e. the 90° Y-type CNT can be installed by pushing approach and pulling approach, respectively. In other words, the force needed during the installation in pushing approach is smaller than that in pulling approach. To illustrate this, two typical configurations of the 90° Y-type CNT with $\Delta R = 4.864$ Å, as shown in Figs. 8*a* and *b*, are taken at the displacements corresponding to the peaks in the loading/unloading processes. It can be found that the two installation methods have different action modes and the deformation of the 90° Y-type CNT in pushing approach is larger than that in pulling approach. Therefore, the pushing approach allows a larger adaptive deformation of the 90° Y-type CNT and sequentially reduces the installation resistance.

Except for the fixed mode similar to the common Y-type CNT, the 90° Y-type CNT has another typical morphology, considered as a T-type CNT, i.e. the branch CNT terminates the inserting end of the trunk CNT. Also, a series of simulations with different gaps are conducted to test the service performance of the proposed T-type CNT. Unfortunately, the terminated inserting end makes the installation not as easy as the Y-type CNTs. To illustrate this, two typical configurations of the T-type CNT in the case of $\Delta R = 3.864$ Å are shown in Fig. 9. The attraction between the

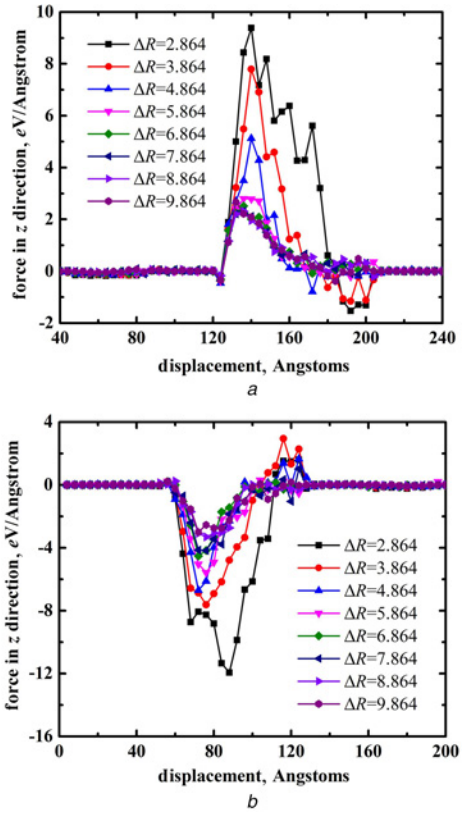

Fig. 7 *Axial force of the 90° Y-type CNT as a function of the displacement in the*
a Loading processes
b Unloading processes

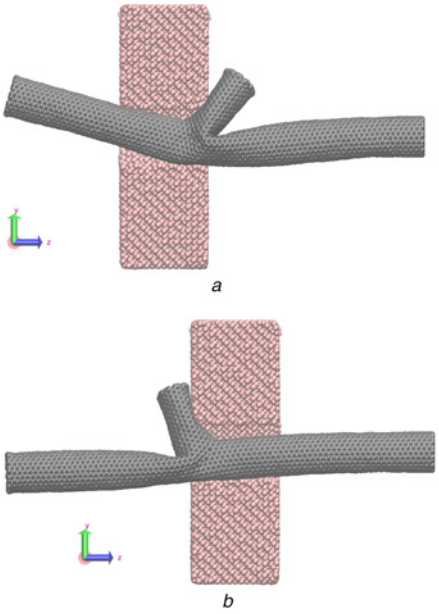

Fig. 8 *Configuration of the 90° Y-type CNT with ΔR = 4.864 Å at the displacement of*
a 140 Å in the loading process
b 72 Å in the unloading process

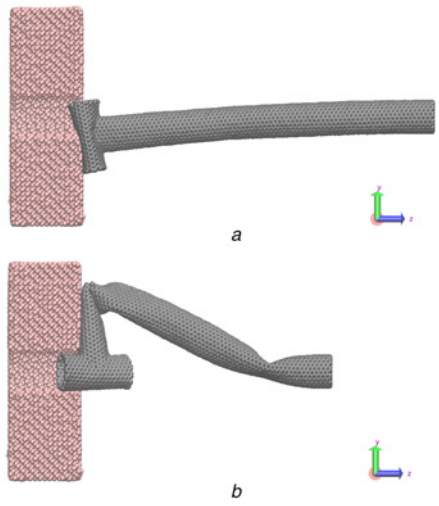

Fig. 9 *Configuration of the T-type CNT with ΔR = 3.864 Å at the moving displacement of*
a 44 Å and
b 100 Å in the loading process

silicon hole and the T-type CNT can mislead the branch (see Fig. 9*a*), and consequently result in the failure installation of the T-type CNT (see Fig. 9*b*). Moreover, with the gaps ranging from 4.864 to 10.864 Å, the force–displacement curves of the T-type CNT in the loading/unloading processes are shown in Fig. 10. Interestingly, the unloading force of the T-type CNT with the smaller gaps ($\Delta R = 4.864$ and 5.864 Å) is distinctly larger than the installation resistance, while this phenomenon is not evident in other cases ($\Delta R \geq 6.864$ Å). To address this, the unloading processes are further observed and the configuration of the T-type CNT at the displacement of 152 Å in the case of $\Delta R = 4.864$ Å is

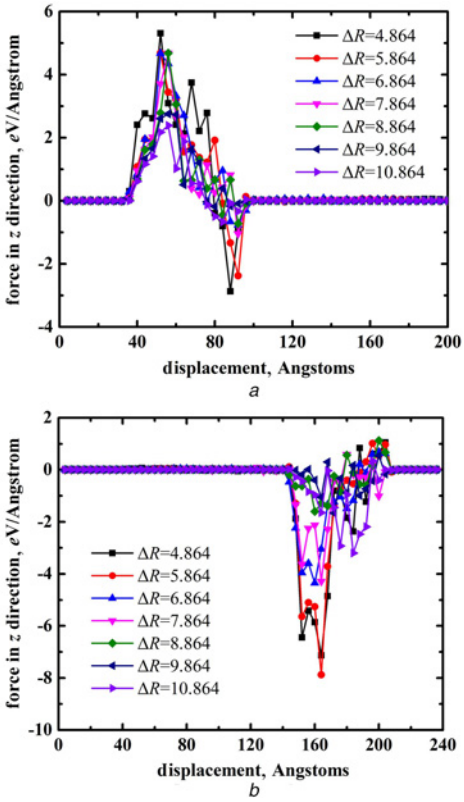

Fig. 10 *Axial force of the T-type CNT as a function of the displacement in the*
a Loading processes
b Unloading processes

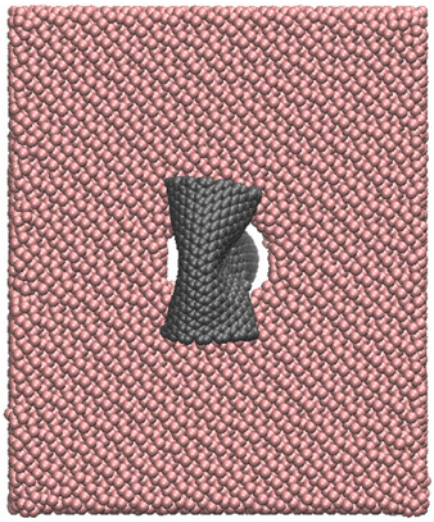

Fig. 11 *Branch of the T-type CNT has an approximately symmetrical structure at the displacement of 152 Å in the case of ΔR = 4.864 Å*

taken as the typical. As shown in Fig. 11, an approximately symmetrical structure emerges on the branch tube of the T-type CNT during the unloading process, acting as a baffle, and thus the fixity of the T-type CNT is greatly enhanced.

doi: 10.1049/mnl.2017.0188

4. Conclusions: In summary, the service performance of the nanopins based on four typical structured CNTs is briefly examined in the loading/unloading processes by using MD simulations. The results show that the Y-type CNT has the highest cost-performance ratio and the great potential in fixity. Although the V-type CNT cannot fasten the hole parts on their own, it can be used cooperatively with another nanopin. The installation resistance and the unloading force are in the same order of magnitude for the 90° Y-type CNT, the installation in pushing approach is easier than that in pulling approach. Moreover, it is difficult for the proposed T-type CNT to be installed owing to the misleading attraction between the silicon hole and the branch CNT, although it is expected to effectively avoid mutual interference in practice. Importantly, several special microstructures occurred on different structured CNTs in loading/unloading process can influence the service performance of the proposed nanopins. The findings may be helpful to design and manufacturing of the CNT-based nanoapparatus.

5. Acknowledgements: This work was supported by the National Natural Science Foundation of China (11472117, 11372298, 51675236 and 11672063). The molecular dynamics simulations were partially supported by Shanghai Supercomputer Center.

6. References

[1] Zhang Z.Q., Zhong J., Ye H.F., *ET AL.*: 'Structural optimization and shear performances of the nanopins based on Y-junction carbon nanotubes', *Physica B*, 2016, **504**, pp. 13–22
[2] Binnig G., Rohrer H., Gerber C., *ET AL.*: '7 × 7 reconstruction on Si(111) resolved in real space', *Phys. Rev. Lett.*, 1983, **50**, (2), pp. 120–123
[3] Ming F.F., Wang K., Pan S., *ET AL.*: 'Assembling and disassembling Ag clusters on Si(111)-(7 × 7) by vertical atomic manipulation', *ACS Nano*, 2011, **5**, (9), pp. 7608–7616
[4] Emmrich M., Schneiderbauer M., Huber F., *ET AL.*: 'Force field analysis suggests a lowering of diffusion barriers in atomic manipulation due to presence of STM tip', *Phys. Rev. Lett.*, 2015, **114**, (14), pp. 146101
[5] Nishi R., Miyagawa D., Seino Y., *ET AL.*: 'Non-contact atomic force microscopy study of atomic manipulation on an insulator surface by nanoindentation', *Nanotechnology*, 2006, **17**, (7), pp. S142–S147
[6] Sakulsermsuk S., Sloan P.A., Palmer R.E.: 'A new mechanism of atomic manipulation: bond-selective molecular dissociation via thermally activated electron attachment', *ACS Nano*, 2010, **4**, (12), pp. 7344–7348
[7] Ming F.F., Zhong G.H., Liu Q., *ET AL.*: 'Probing the generalized magicity of Ag nanoclusters constructed on Si(111) by atomic manipulation', *Phys. Rev. B*, 2013, **88**, (12), pp. 125432
[8] Sloan P.A., Palmer R.E.: 'Two-electron dissociation of single molecules by atomic manipulation at room temperature', *Nature*, 2005, **434**, (7031), pp. 367–371
[9] Schuler B., Fatayer S., Mohn F., *ET AL.*: 'Reversible Bergman cyclization by atomic manipulation', *Nat. Chem.*, 2016, **8**, (3), pp. 220–224
[10] Breen T.L., Tien J., Oliver S.R., *ET AL.*: 'Design and self-assembly of open, regular, 3D mesostructures', *Science*, 1999, **284**, (5416), pp. 948–951
[11] Brinker C.J., Lu Y.F., Sellinger A., *ET AL.*: 'Evaporation-induced self-assembly: nanostructures made easy', *Adv. Mater.*, **11**, (1999), pp. 579–585
[12] Rabani E., Reichman D.R., Geissler P.L., *ET AL.*: 'Drying-mediated self-assembly of nanoparticles', *Nature*, 2003, **426**, (6964), pp. 271–274
[13] Wang D.R., Wang X.G.: 'Amphiphilic azo polymers: molecular engineering, self-assembly and photo responsive properties', *Prog. Polym. Sci.*, 2013, **38**, (2), pp. 271–301
[14] Cui H.G., Muraoka T., Cheetham A.G., *ET AL.*: 'Self-assembly of giant peptide nanobelts', *Nano Lett.*, 2009, **9**, (3), pp. 945–951
[15] Yan D.Y., Zhou Y.F., Hou J.: 'Supramolecular self-assembly of macroscopic tubes', *Science*, 2004, **303**, (5654), pp. 65–67
[16] Darling S.B.: 'Directing the self-assembly of block copolymers', *Prog. Polym. Sci.*, 2007, **32**, (10), pp. 1152–1204
[17] Lynd N.A., Meuler A.J., Hillmyer M.A.: 'Polydispersity and block copolymer self-assembly', *Prog. Polym. Sci.*, 2008, **33**, (9), pp. 875–893
[18] Klok H.A., Lecommandoux S.: 'Supramolecular materials via block copolymer self-assembly', *Adv. Mater.*, 2001, **13**, (16), pp. 1217–1229
[19] Rosen B.M., Wilson C.J., Wilson D.A., *ET AL.*: 'Dendron-mediated self-assembly, disassembly, and self-organization of complex systems', *Chem. Rev.*, 2009, **109**, (11), pp. 6275–6540
[20] Ikkala O., Ten B.G.: 'Hierarchical self-assembly in polymeric complexes: towards functional materials', *Chem. Commun.*, 2004, **19**, (19), pp. 2131–2137
[21] Jonkheijm P., Schoot P.V.D., Schenning A.P.H.J., *ET AL.*: 'Probing the solvent-assisted nucleation pathway in chemical self-assembly', *Science*, 2006, **313**, (5783), pp. 80–83
[22] Williams R.J., Smith A.M., Collins R., *ET AL.*: 'Enzyme-assisted self-assembly under thermodynamic control', *Nat. Nanotechnol.*, 1991, **4**, (3), pp. 19–24
[23] Karaborni S., Esselink K., Hilbers P.A.J., *ET AL.*: 'Simulating the self-assembly of gemini (dimeric) surfactants', *Science*, 1994, **266**, (5183), pp. 254–256
[24] Harada A., Kobayashi R., Takashima Y., *ET AL.*: 'Macroscopic self-assembly through molecular recognition', *Nat. Chem.*, 2011, **3**, (1), pp. 34–37
[25] Cho W.D., Schulz M., Shanov V.: 'Growth and characterization of vertically aligned centimeter long CNT arrays', *Carbon*, 2014, **72**, (7), pp. 264–273
[26] Lin Q.F., Hua B., Leung S.F., *ET AL.*: 'Efficient light absorption with integrated nanopillar/nanowell arrays for three-dimensional thin-film photovoltaic applications', *ACS Nano*, 2013, **7**, (3), pp. 2725–2732
[27] Nagase M., Hibino H., Kageshima H., *ET AL.*: 'In-plane conductance measurement of graphene nanoislands using an integrated nanogap probe', *Nanotechnology*, 2008, **19**, (49), pp. 495701
[28] Yanik A.A., Huang M., Artar A., *ET AL.*: 'Integrated nanoplasmonic-nanofluidic biosensors with targeted delivery of analytes', *Appl. Phys. Lett.*, 2010, **96**, (2), pp. 021101
[29] Shulaker M.M., Hills G., Patil N., *ET AL.*: 'Carbon nanotube computer', *Nature*, 2013, **501**, (7468), pp. 526–530
[30] Kang J.W., Hwang H.J.: 'Nanoscale carbon nanotube motor schematics and simulations for micro-electro-mechanical machines', *Nanotechnology*, 2004, **15**, (11), pp. 1633–1638
[31] Kan B., Ding J.N., Zhang Y.B., *ET AL.*: 'A nanoscale transmission system with novel-structured carbon nanotubes', *J. Appl. Phys.*, 2013, **113**, (1), pp. 014310
[32] Choi S.H., Lee J.H., Kang Y.C.: 'Perforated metal oxide-carbon nanotube composite microspheres with enhanced lithium-ion storage properties', *ACS Nano*, 2015, **9**, (10), pp. 10173–10185
[33] Prosini P.P., Pozio A., Botti S., *ET AL.*: 'Electrochemical studies of hydrogen evolution, storage and oxidation on carbon nanotube electrodes', *J. Power Sources*, 2003, **118**, (1), pp. 265–269
[34] Zhang Z.Q., Zhang H.W., Zheng Y.G., *ET AL.*: 'Gas separation by kinked single-walled carbon nanotubes: Molecular dynamics simulations', *Phys. Rev. B*, 2010, **78**, (3), pp. 035439
[35] Chen H.Y., Liu Z.F., Gong X.G., *ET AL.*: 'Design of a one-way nanovalve based on carbon nanotube junction and C60', *Microfluid. Nanofluid.*, 2011, **10**, (4), pp. 927–933
[36] Zhang Z.Q., Ye H.F., Liu Z., *ET AL.*: 'Carbon nanotube-based charge-controlled speed-regulating nanoclutch', *J. Appl. Phys.*, 2012, **111**, (11), pp. 114304
[37] Li C.Y., Chou T.W.: 'Elastic moduli of multi-walled carbon nanotubes and the effect of van der Waals forces', *Compos. Sci. Technol.*, 2003, **63**, (11), pp. 1517–1524
[38] Zang J.L., Yuan Q.Z., Wang F.C., *ET AL.*: 'A comparative study of Young's modulus of single-walled carbon nanotube by CPMD, MD and first principle simulations', *Comp. Mater. Sci.*, 2009, **46**, (3), pp. 621–625
[39] Zhao Y.P.: 'Nano and Mesoscopic Mechanics' (Science Press, Beijing, 2014), Chapter one
[40] Zhang Z.Q., Zhong J., Ye H.F., *ET AL.*: 'A novel nanopin model based on a Y-junction carbon nanotube', *J. Appl. Phys.*, 2016, **120**, (6), pp. 064301
[41] Saito R., Matsuo R., Kimura T., *ET AL.*: 'Anomalous potential barrier of double-wall carbon nanotube', *Chem. Phys. Lett.*, 2001, **348**, (3), pp. 187–193
[42] Yu N., Polycarpou A.A.: 'Adhesive contact based on the Lennard-Jones potential: a correction to the value of the equilibrium distance as used in the potential', *J. Colloid Interf. Sci.*, 2004, **278**, (2), pp. 428–435
[43] Bellido E.P., Seminario J.M.: 'Molecular dynamics simulations of folding of supported graphene', *J. Phys. Chem. C*, 2010, **114**, (51), pp. 22472–22477